Data report: major and trace element composition of silicates and carbonates from Bengal Fan sediments, IODP Expedition 354[1]

Aswin Pradeep Tachambalath[2], Christian France-Lanord[2], Albert Galy[2], Thomas Rigaudier[2], and Julien Charreau[2]

Contents

Keywords

References (RIS)

Abstract

During International Ocean Discovery Program Expedition 354, seven sites were drilled along a 320 km east–west transect at 8°N, constituting a relic of the Neogene sediment record of Himalayan erosion. Bengal Fan is one of the largest deep-sea fans in the world where turbiditic sediments issued from the Ganga and Brahmaputra River Delta and originally supplied by the Himalayan erosion of silicate and carbonate lithologies are deposited and stored. Quantification of the chemical composition of silicates and carbonates is necessary to understand the tectonoclimatic history of this region. This report presents the major and trace element concentrations of silicate and carbonate fractions of selected turbiditic samples from Sites U1450 and U1451. Efficient washing followed by refined acid leaching of the sediments was performed to eliminate sea salts and carbonates from these marine sediment samples. Shipboard samples show 20%–40% excess sodium concentration associated with sea salt derived from pore water. Weak acid treatment limits the total carbonate content in the samples to less than 0.1%. Depletion of major and trace elements observed due to acid leaching is attributed to the dissolution of carbonates and cations associated with Fe-Mn oxyhydroxides.

1. Introduction

International Ocean Discovery Program (IODP) Expedition 354 (**France-Lanord et al.**, 2016a) explored the Bengal Fan through a 320 km east–west transect of seven sites cored at 8°N, allowing the production of a Neogene record of the Himalayan erosion. Bengal Fan sediments are mainly composed of turbidites issued from the Ganga and Brahmaputra River Delta supplied by the Himalayan erosion of silicate and carbonate lithologies. The quantification of the chemical composition of silicates and carbonates is necessary to address various questions such as the source of the sediments, the mineralogical composition, the transport sorting processes, or the chemical weathering and diagenetic evolution. However, the partitioning of major cations between silicates and carbonates sources is exacerbated because calcium and magnesium ions are both major elements of silicates and carbonates. In addition, salts left by residual pore water contribute to a significant proportion of the sodium concentration. This implies developing chemical treatments to sort out the contributions of sea salt and carbonates to the whole rock composition. This includes water washing for sea salts and acid leaching to eliminate the carbonates (e.g., France-Lanord and Derry, 1997; Bickle et al., 2015; Rapuc et al., 2021).

Here, we report major and trace element composition of the silicate fraction and the carbonate concentrations of selected turbidite samples of the Bengal Fan collected during Expedition 354. We compare three different analytical processes for the same sample set: (1) shipboard analyses on bulk samples with no other treatments than grinding (**France-Lanord et al.**, 2016b), (2) analyses of water-washed samples, and (3) analyses of acetic acid leached samples. These allow estimations of silicate and carbonate composition.

2. Materials and methods

This study reports the major and trace element composition of 33 turbiditic samples from Sites U1450 and U1451. Hole U1450A was drilled to 687.4 meters below seafloor (mbsf), and Hole U1450B was drilled without recovery to 608 mbsf and cored from 608 to 811.9 mbsf (**France-Lanord et al.**, 2016b). Samples from Hole U1451A were selected from near the seabed to 337.52 mbsf. The samples span an age from late Miocene to recent (**Lenard et al.**, 2020; Cruz et al., 2021). The sample set was selected and prepared during Expedition 354. Further laboratory washing and acetic acid leaching processing were conducted on fractions of the same powdered samples.

2.1. Water washing

A triple-washing process was employed to remove sea salt from the selected samples. The sediments were washed three times with deionized water, with a water to sediment ratio of 1:10. At each step, sediments were separated from water using a 90 mm polyethersulfone 0.2 μm filter. The filtered sediments were then freeze-dried and homogenized.

2.2. Acetic acid leaching

A weak acid (dilute acetic acid) treatment was applied to the sediment samples to eliminate the carbonates. The use of acetic acid compared to strong acids like hydrochloric acid minimizes the risk of alteration and oxidation of elements occurring during the leaching process, and the crystallinity of the silicate minerals is preserved (Poppe et al., 2001). Acetic acid is more efficient at dissolving the calcites than dolomites for a given amount of time (Ray et al., 1957); therefore, care must be taken to control the complete decarbonation of the sample. The decarbonation procedure is described below:

1. Weigh approximately 0.5 g of sediment in a 50 mL centrifuge tube.
2. Mix the sediment with 30–35 mL of 20% (v/v) of glacial acetic acid and subject to intermittent ultrasonic treatment and vortex agitation for 20 min, thereby facilitating thorough mixing of acetic acid solution with the sediment.
3. Loosen the lids of the centrifuge tube to remove the CO_2 generated by the acid reacting with the carbonates present in the sample.
4. Centrifuge and remove the supernatant (leachate).
5. Wash the residue with 35 mL Milli-Q water and freeze-dry.

The sediments were decarbonated to bring the carbonate content to less than 0.1% (equivalent $CaCO_3$ wt%). The completeness of the decarbonation was controlled by analyzing the remaining carbonate concentration. A summary diagram displaying the treatment steps for efficient decarbonation of the samples is shown in Figure **F1**.

Bulk sample (without water washing) analyses for major and selected trace elements were performed during the expedition (see Table **T14** in the Site U1450 chapter [France-Lanord et al., 2016b]). The bulk carbonate content was measured using a coulometric technique (see Table **T13** in the Site U1450 chapter [France-Lanord et al., 2016b]).

For washed and decarbonated samples, the major and trace element concentrations were measured using inductively coupled plasma–atomic emission spectroscopy (ICP-AES) and inductively coupled plasma–mass spectrometry (ICP-MS), respectively, at the Service d'Analyse de Roche et des Minéraux (SARM). Loss on ignition was determined by mass loss after calcination of ~200 mg of homogenized samples at 1020°C for 6 h. The anhydrous residue was fused with lithium

metaborate ($LiBO_2$) and dissolved in nitric acid prior to analysis using inductively coupled plasma spectroscopy (ICP) (Carignan et al., 2001). Analytical uncertainties vary from <2% for SiO_2 to 20% for MnO_2, depending on the concentrations.

Carbonate concentrations on the washed samples and leaching tests were determined with stable isotope techniques using an automatic carbonate to CO_2 preparation system (Thermo Scientific GasBench) coupled with a Thermo Scientific MAT 253 Isotope Ratio Mass Spectrometer (Table **T1**). For each washed sample, 5–10 mg of homogenized powder was treated with 0.5 mL of supersaturated orthophosphoric acid at 70°C for approximately 10 h under a helium atmosphere. A leaching control test was performed on 30–40 mg of homogenized powder. The area of the $^{44}CO_2$ signal was calibrated by using pure Merck calcite standards and three internal standards of Himalayan River sediments containing 3–17 wt% carbonates composed of a mixture of calcite and dolomite. Standards were measured after every seven samples to improve the calibration. Accuracy is better than 5%.

3. Results

Major element concentrations of the washed and decarbonated sediments are reported in Tables **T1** and **T2** respectively. The sediments span a relatively large variation in concentrations due to the mineralogical and grain size sorting during turbiditic transport. For a given element, the amount of removal due to acetic acid leaching can be estimated by using a mass balance calculation, assuming that the leaching mobility of aluminum is negligible. This is assessed by analysis of Al loss during acetic acid leaching of Himalayan River sediments by Bickle et al. (2015), which
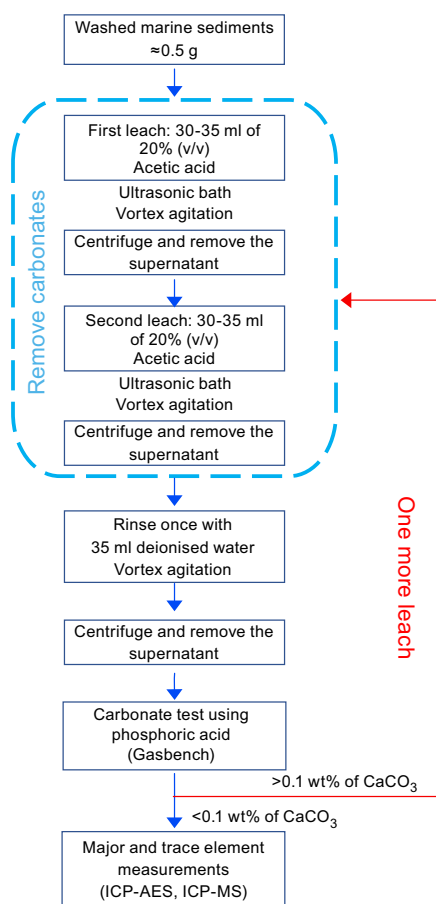

Figure F1. Acetic acid leaching protocol for efficient decarbonation of marine sediments.

Table T1. Washed sample major element concentrations, Sites U1450 and U1451. **Download table in CSV format.**

ranges 0.4%–2% of the total aluminum,. This lies within the range of analytical uncertainty of Al (<2%). Therefore, the loss of a given element during the leaching step can be expressed with the following equation:

$$\Delta X = [X]_{washed} - \frac{[X]_{decarbonated}}{[Al]_{decarbonated}} \times [Al]_{washed},$$

where ΔX represents the molar concentration of element X in the washed sample removed by leaching. $[X]_{washed}$ and $[X]_{decarbonated}$ represent the molar concentration of the considered element in the washed and decarbonated fractions.

3.1. Effect of sea salt removal

The water washing process is critical for Na concentration. A comparison of shipboard analyses and the washed samples analyses (Figure **F2**) clearly reflects the presence of excess Na in the shipboard data. Sea salt derived from pore water contributes to 20%–40% of the bulk sodium concentration. Effects of washing on the concentration of other major and trace elements are negligible, and the variations lie within the analytical uncertainty.

3.2. Effect of acid leaching on silicate major element and trace element concentrations

To assess the action of leaching on the major element concentrations of the sediments ([X]), a comparison between Al-normalized concentrations of washed samples ($[X/Al]_{washed}$) and decarbonated samples ($[X/Al]_{decarbonated}$) is presented with respect to a 1:1 line (Figure **F3**). Comparison of Na concentrations (Figure **F3A**) between the washed and decarbonated samples shows a depletion (10%–23%) of Na in a few samples, indicating incomplete removal of sea salt even after the routine washing procedure. Regression analysis of these data ($n = 33$; $r^2 = 0.94$; $p < 0.05$; y = {0.99 ± 0.04}x + {−0.01 ± 0.01}) indicates a statistically significant correlation between the decarbonated and washed Na/Al ratios, and the intercept of the regression is within the uncertainty of zero.

Unlike Na/Al variations, the changes in K/Al ratios of the decarbonated samples (Figure **F3B**) are within the range of analytical uncertainties, indicating negligible loss of potassium due to the mild acetic acid treatment. Variations in titanium concentrations in decarbonated samples compared to the washed samples lie within the analytical uncertainties (Figure **F3F**), indicating negligible loss of titanium during decarbonation.

Table T2. Major and trace element concentrations in decarbonated samples, Sites U1450 and U1451. **Download table in CSV format.**
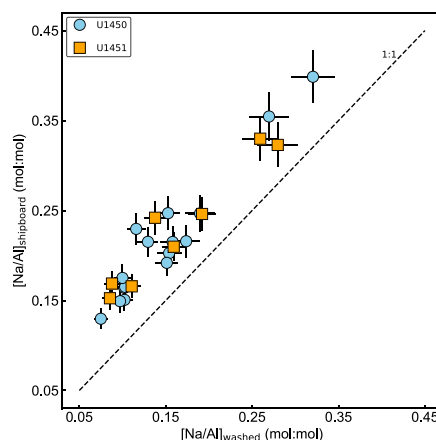

Figure F2. Comparison of Na (normalized to Al) concentration of shipboard samples to washed samples, Sites U1450 and U1451. Error bars = analytical uncertainties associated with Al-normalized ratios. Dashed line = 1:1 line.

Major loss of calcium and magnesium is observed, representing 30%–90% and 7%–43% of bulk concentration, respectively (Figure **F3C, F3D**). These are linked to the contribution of carbonates, including both calcite and dolomite. Mild acid treatment does not show a systematic variation in Si/Al ratios (Figure **F3H**). Both depletion (2%–15%) and enrichment in the Si concentrations are observed for a few samples. Regression analyses indicate a statistically strong correlation between
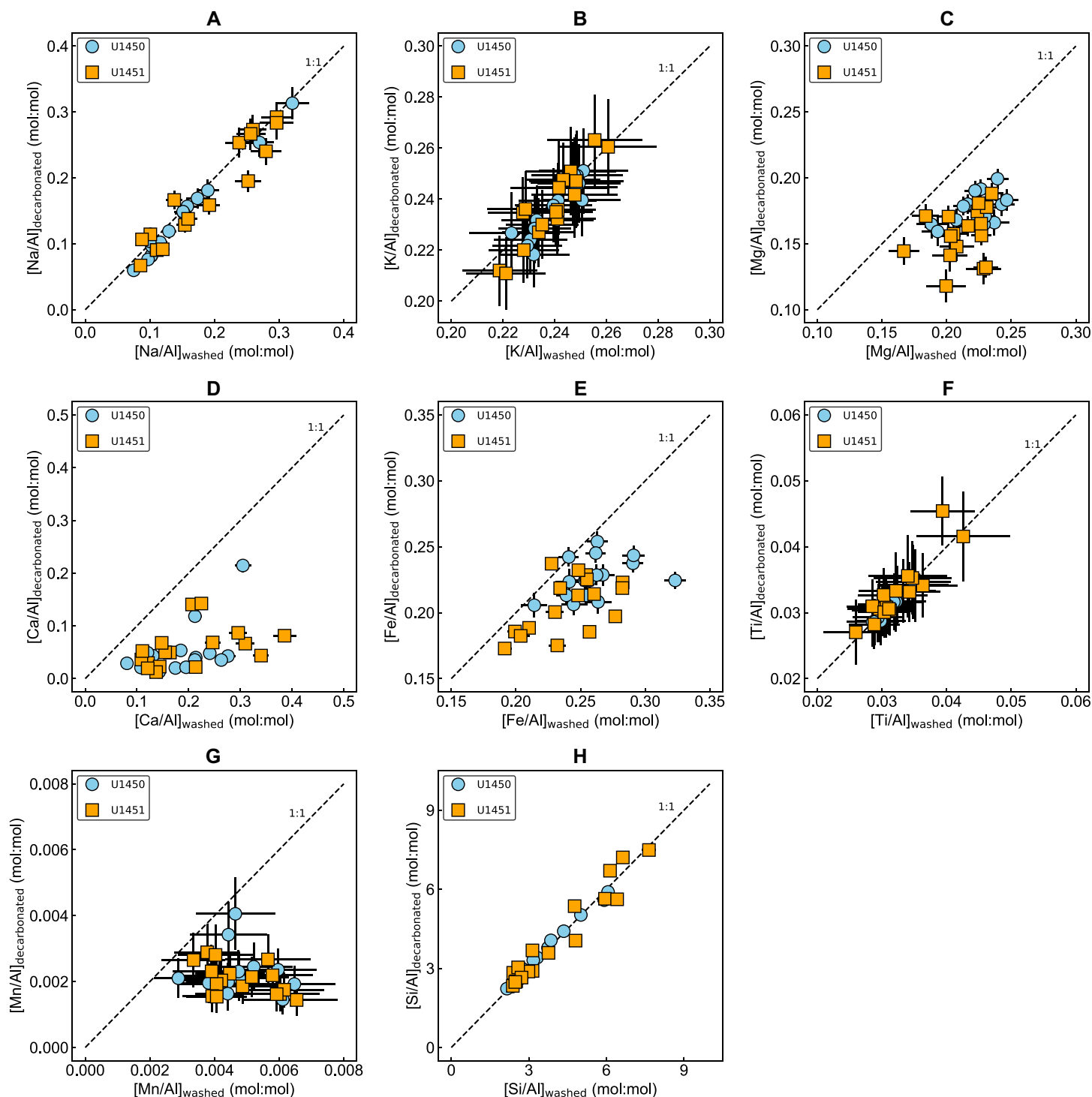

Figure F3. A–H. Comparison of washed and decarbonated major element concentrations normalized to aluminum, Sites U1450 and U1451. Error bars = analytical uncertainties associated with the Al-normalized ratios. Regression analysis of (A) Na ($n = 33$; $r^2 = 0.94$; $p < 0.05$; y = {0.99 ± 0.04}x + {−0.01 ± 0.01}) and (H) Si ($n = 33$; $r^2 = 0.95$; $p < 0.05$; y = {0.96 ± 0.04}x + {0.02 ± 0.15}) indicate negligible loss of sodium and silicon due to acetic acid leaching.

decarbonated and the washed Si/Al ratios (n = 33; r^2 = 0.95; p < 0.05; y = {0.96 ± 0.04}x + {0.02 ± 0.15}).

A significant loss of iron (10%–30%) and manganese (12%–77%) is observed during acetic acid leaching (Figure **F3F, F3G**). The moderate covariation (n = 33; r^2 = 0.61; p < 0.1) between ΔFe and ΔMn (Fe and Mn lost due to acetic acid leaching) indicates that it is likely associated with the removal of Fe-Mn oxyhydroxides during the leaching process (Figure **F4**). It is difficult to confirm whether all the Fe-Mn oxyhydroxides are leached by acetic acid treatment. The ratio of leached Mn to leached Fe (ΔMn/ΔFe) varies from 0.03 to 0.21 (n = 31) with an average value of 0.07.

Acetic acid is reported to be more efficient in the dissolution of some Mn oxyhydroxides (not all) and less effective in mobilizing Fe oxyhydroxide phases (Gourlan et al., 2010; Wilson et al., 2013; Blaser et al., 2016). Hence, the depletion in the iron observed could also be due to the dissolution of terrigenous iron oxides. Two samples show a relative enrichment in iron concentrations resulting from decarbonation and negative values of ΔFe.

Phosphate concentrations in the decarbonated samples are below the detection limit for most of the samples (n = 30) and hence are not shown in Figure **F3**. Dissolution of phosphate associated with carbonates and heavy minerals like apatite could result in loss of phosphate in an acetic acid medium.

3.3. Effect of acetic acid leaching on trace element concentrations

Strontium and neodymium are key trace elements because their concentrations and isotopic compositions are useful tracers for source identification (e.g., Galy et al., 1996; France-Lanord and Derry, 1997; Goodbred et al., 2014; Galy et al., 2008; **Lenard et al.**, 2020). Strontium shows a significant loss (3%–67%) with decarbonation (Figure **F5A**). The moderate correlation (n = 33; r^2 = 0.47; p < 0.01) of the ΔSr with (ΔCa + ΔMg) indicates the clear association of strontium with carbonates (Figure **F5B**).

Unlike strontium, the effect of leaching on neodymium is not systematic (Figure **F6**). Some samples show negligible loss of Nd (within the analytical uncertainty), whereas 9 out of 33 samples show loss of 10%–24% of the [Nd]$_{washed}$. The Nd linked to the leached iron associated with iron oxyhydroxides may explain the depletion in Nd concentrations, resulting from decarbonation.

Trace elements lead and copper show depletions of 14%–54% and 21%–68%, respectively, due to acetic acid leaching (Figure **F7A, F7B**). Moderate correlations of ΔPb and ΔCu with ΔMn underscore the association of Pb and Cu to manganese oxides (Figure **F7C, F7D**).

The comparison between the washed and decarbonated samples for the sum of rare earth elements (ΣREE) also shows a systematic depletion associated with leaching (Figure **F8**). This obser-
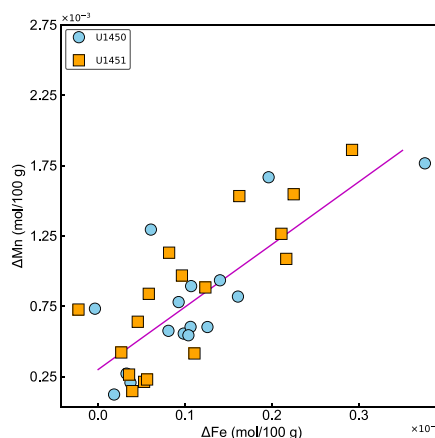

Figure F4. Leached Mn (ΔMn) compared to leached Fe (ΔFe) for selected samples, Sites U1450 and U1451. Regression line (purple color) shows a moderate correlation (n = 33; r^2 = 0.61; p < 0.01) between ΔMn and ΔFe.

vation is coherent with the depletion of phosphate, iron, and manganese, which could result in the dissolution of heavy minerals, Fe-Mn oxyhydroxides, and associated trace elements.

3.4. Carbonate information

A comparison between the molar concentrations of CO_2 from carbonate measured in the washed samples and the molar loss in Ca and Mg ($\Delta Ca + \Delta Mg$) is presented in Figure **F9**. The good correlation confirms that 30%–90% of total Ca and 7%–42% of total Mg in the washed sediment are associated with carbonate phases. The proportions of leached Ca and Mg indicate that the samples contain 0.9%–7.7% calcite and 0.3%–2.8% dolomite.

The decarbonation protocol described above allows us to estimate carbonate and silicate compositions from marine sediment samples. Careful evaluation of the leaching effects confirms that the acetic acid leaching efficiently removes the carbonates, but also partially dissolves Fe-Mn oxides and phosphates. Combining washed and leached analyses, a summary of the silicate and carbonate concentrations of the major elements is given in Table **T3**. Concentrations (in weight percent) of SiO_2, Al_2O_3, Fe_2O_3, K_2O, MnO, and P_2O_5 are representative concentrations derived from the
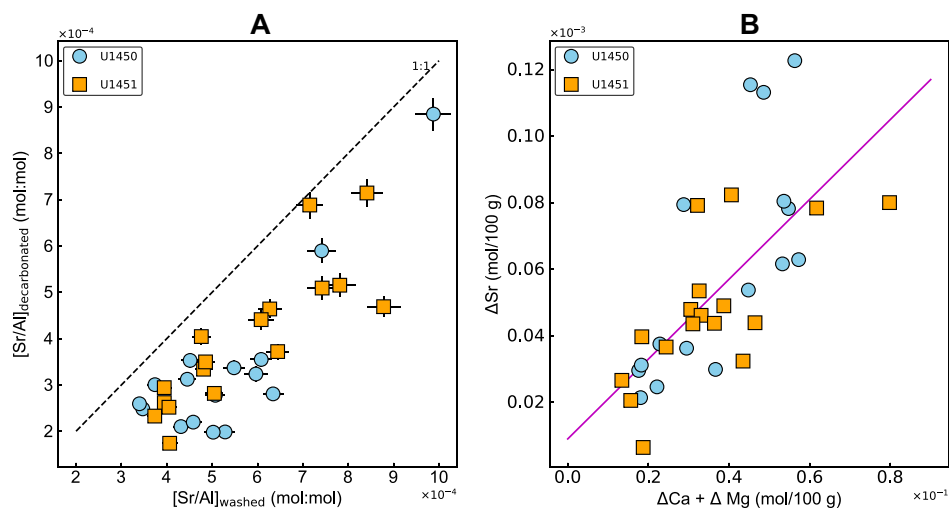

Figure F5. Sr, Sites U1450 and U1451. A. Comparison of Sr (normalized to aluminum) of washed samples to decarbonated samples (dashed line = 1:1 line). B. Moderate correlation (n = 33; r^2 = 0.47; p < 0.01) of leached Sr (ΔSr) to sum of leached calcium and magnesium (ΔCa + ΔMg). Purple line = regression line.
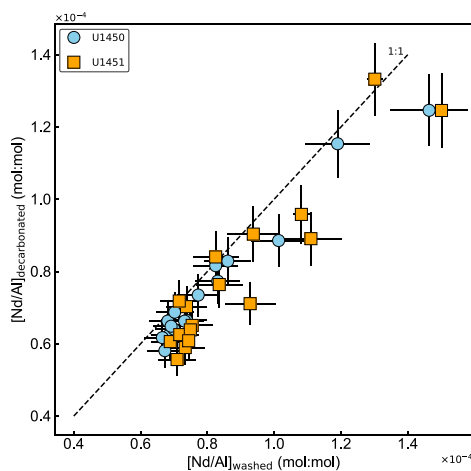

Figure F6. Comparison of Nd/Al ratios in washed samples and decarbonated samples, Sites U1450 and U1451. Error bars = associated analytical uncertainties. Dashed lines = 1:1 line.
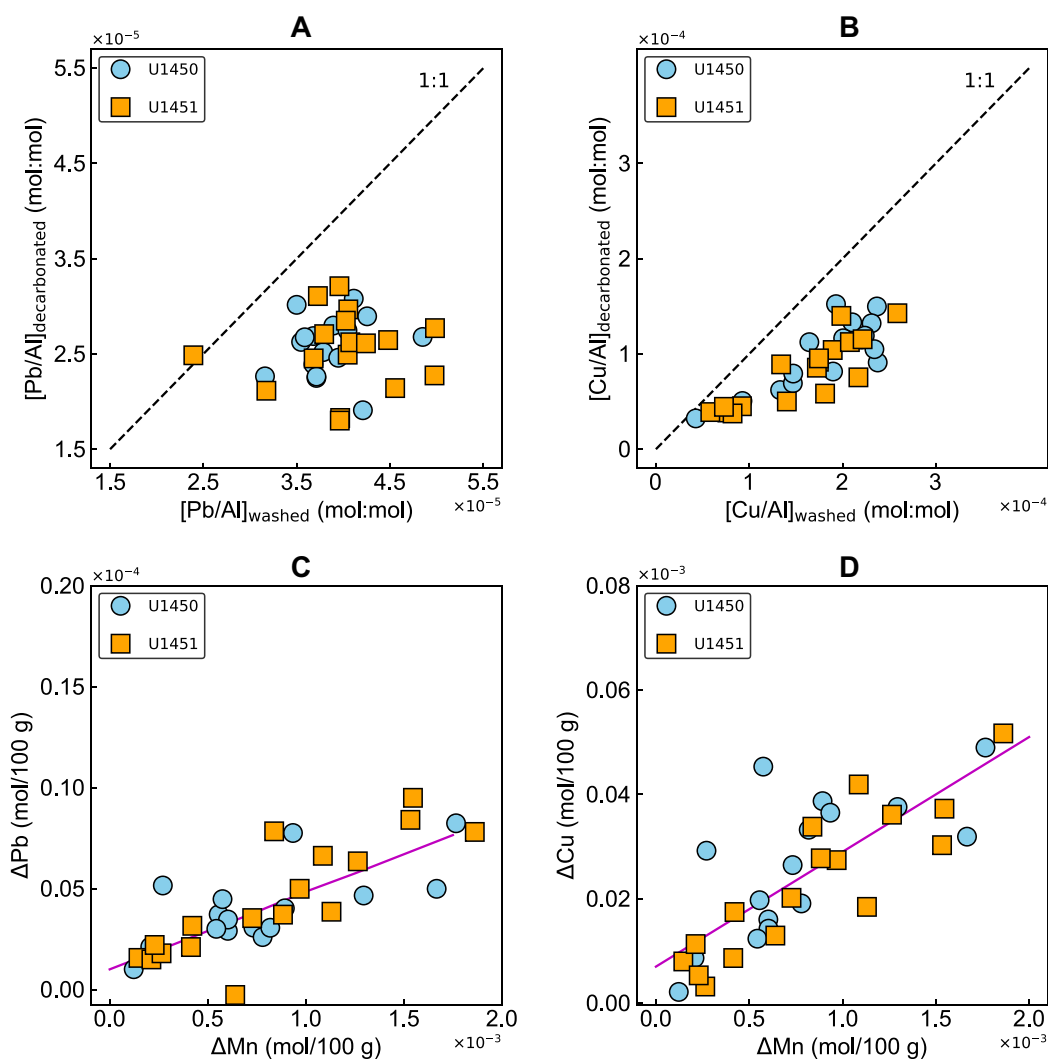
Figure F7. A, B. Comparison of Pb/Al and Cu/Al ratios between washed and decarbonated samples, Sites U1450 and U1451. Dashed line = 1:1 line. C. Moderate correlation ($n = 33$; $r^2 = 0.59$; $p < 0.01$) between leached lead (ΔPb) and leached manganese (ΔMn) concentrations. D. Moderate correlation ($n = 33$; $r^2 = 0.61$; $p < 0.01$) between leached copper (ΔCu) and leached manganese (ΔMn) concentrations. Purple line = regression line.
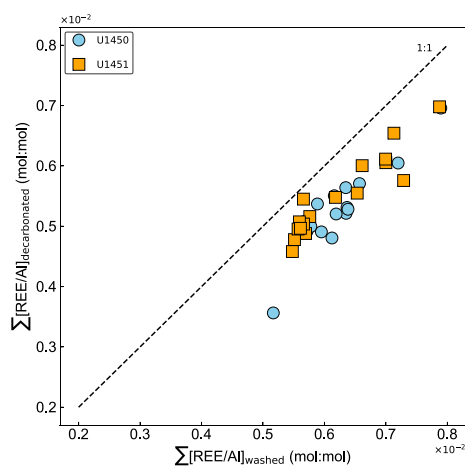

Figure F8. Comparison of washed and decarbonated samples showing impact of acetic acid leaching on sum of all rare earth elements (ΣREE) normalized to aluminum, Sites U1450 and U1451. Dashed line = 1:1 line.
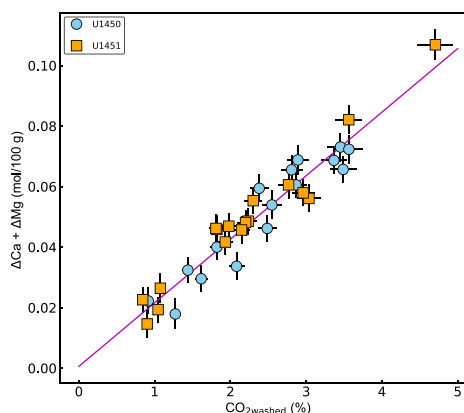
Figure F9. Comparison between CO_2 measured in washed sediments and sum of leached Ca and Mg ($\Delta Ca + \Delta Mg$), Sites U1450 and U1451. Error bars = analytical uncertainties. Purple line = error weighted regression line (y = {0.021 ± 0.001}x + {0 ± 0.002}).

Table T3. Major element concentrations recovered from washing and acetic acid decarbonation of selected samples, Sites U1450 and U1451. **Download table in CSV format.**

washed samples. Silicate and carbonate derived MgO and CaO are calculated using normalization to Al:

$$[X]_{washed} = [X]_{sil} + [X]_{carb}$$

$$= \frac{[X]_{decarbonated}}{[Al]_{decarbonated}} \times [Al]_{washed} + [X]_{carb},$$

$$= \frac{[X]_{decarbonated}}{[Al]_{decarbonated}} \times [Al]_{washed} + \Delta X$$

where [X] = Ca or Mg.

An estimate of the CO_2 derived from the analyzed total carbonate using the automatic carbonate to CO_2 preparation system is denoted as $CO_{2carbonate}$ (Table **T3**). An estimate of the difference in loss on ignition and CO_2 from carbonates is also provided in Table **T3** to make a mass balance on the major element concentrations of the selected samples used in this study.

4. Acknowledgments

References

Bickle, M.J., Tipper, E., Galy, A., Chapman, H., and Harris, N., 2015. On discrimination between carbonate and silicate inputs to Himalayan rivers. American Journal of Science, 315(2):120–166. **https://doi.org/10.2475/02.2015.02**

Blaser, P., Lippold, J., Gutjahr, M., Frank, N., Link, J.M., and Frank, M., 2016. Extracting foraminiferal sea water Nd isotope signatures from bulk deep sea sediment by chemical leaching. Chemical Geology, 439:189–204. **https://doi.org/10.1016/j.chemgeo.2016.06.024**

Carignan, J., Hild, P., Mevelle, G., Morel, J., and Yeghicheyan, D., 2001. Routine analyses of trace elements in geological samples using flow injection and low pressure on-line liquid chromatography coupled to ICP-MS: a study of geochemical feference materials BR, DR-N, UB-N, AN-G and GH. Geostandards Newsletter, 25(2–3):187–198. **https://doi.org/10.1111/j.1751-908X.2001.tb00595.x**

Cruz, J.W., Wise, S.W., Jr., and Parker, W.C., 2021. Miocene to Recent calcareous nannofossil biostratigraphy in the eastern Bengal Fan (Indian Ocean): linking turbidites to tectonic activity during the evolution of the Himalayas. Journal of Nannoplankton Research, 39(1):15–28.

http://ina.tmsoc.org/JNR/online-early/39/Cruz%20et%20al%202021%20JNR%20Neogene%20Indian%20Ocean%20IODP%20site%201451.pdf

France-Lanord, C., Spiess, V., Klaus, A., Schwenk, T., Adhikari, R.R., Adhikari, S.K., Bahk, J.-J., Baxter, A.T., Cruz, J.W., Das, S.K., Dekens, P., Duleba, W., Fox, L.R., Galy, A., Galy, V., Ge, J., Gleason, J.D., Gyawali, B.R., Huyghe, P., Jia, G., Lantzsch, H., Manoj, M.C., Martos Martin, Y., Meynadier, L., Najman, Y.M.R., Nakajima, A., Ponton, C., Reilly, B.T., Rogers, K.G., Savian, J.F., Selkin, P.A., Weber, M.E., Williams, T., and Yoshida, K., 2016a. Expedition 354 summary. In France-Lanord, C., Spiess, V., Klaus, A., Schwenk, T., and the Expedition 354 Scientists, Bengal Fan. Proceedings of the International Ocean Discovery Program, 354: College Station, TX (International Ocean Discovery Program). https://doi.org/10.14379/iodp.proc.354.101.2016

France-Lanord, C., Spiess, V., Klaus, A., Adhikari, R.R., Adhikari, S.K., Bahk, J.-J., Baxter, A.T., Cruz, J.W., Das, S.K., Dekens, P., Duleba, W., Fox, L.R., Galy, A., Galy, V., Ge, J., Gleason, J.D., Gyawali, B.R., Huyghe, P., Jia, G., Lantzsch, H., Manoj, M.C., Martos Martin, Y., Meynadier, L., Najman, Y.M.R., Nakajima, A., Ponton, C., Reilly, B.T., Rogers, K.G., Savian, J.F., Schwenk, T., Selkin, P.A., Weber, M.E., Williams, T., and Yoshida, K., 2016b. Site U1450. In France-Lanord, C., Spiess, V., Klaus, A., Schwenk, T., and the Expedition 354 Scientists, Bengal Fan. Proceedings of the International Ocean Discovery Program, 354: College Station, TX (International Ocean Discovery Program). https://doi.org/10.14379/iodp.proc.354.104.2016

France-Lanord, C., and Derry, L.A., 1997. Organic carbon burial forcing of the carbon cycle from Himalayan erosion. Nature, 390(6655):65–67. https://doi.org/10.1038/36324

Galy, A., France-Lanord, C., and Derry, L.A., 1996. The late Oligocene-early Miocene Himalayan belt constraints deduced from isotopic compositions of early Miocene turbidites in the Bengal Fan. Tectonophysics, 260(1–3):109–118. https://doi.org/10.1016/0040-1951(96)00079-0

Galy, V., François, L., France-Lanord, C., Faure, P., Kudrass, H., Palhol, F., and Singh, S.K., 2008. C4 plants decline in the Himalayan basin since the Last Glacial Maximum. Quaternary Science Reviews, 27(13–14):1396–1409. https://doi.org/10.1016/j.quascirev.2008.04.005

Goodbred, S.L., Jr., Paolo, P.M., Ullah, M.S., Pate, R.D., Khan, S.R., Kuehl, S.A., Singh, S.K., and Rahaman, W., 2014. Piecing together the Ganges-Brahmaputra-Meghna River delta: use of sediment provenance to reconstruct the history and interaction of multiple fluvial systems during Holocene delta evolution. Geological Society of America Bulletin, 126(11–12):1495–1510. https://doi.org/10.1130/B30965.1

Gourlan, A.T., Meynadier, L., Allègre, C.J., Tapponnier, P., Birck, J.-L., and Joron, J.-L., 2010. Northern Hemisphere climate control of the Bengali rivers discharge during the past 4 Ma. Case studies of neodymium isotopes in paleoceanography, 29(19–20):2484–2498. https://doi.org/10.1016/j.quascirev.2010.05.003

Lenard, S.J.P., Cruz, J., France-Lanord, C., Lavé, J., and Reilly, B.T., 2020. Data report: calcareous nannofossils and lithologic constraints on the age model of IODP Site U1450, Expedition 354, Bengal Fan. In France-Lanord, C., Spiess, V., Klaus, A., Schwenk, T., and the Expedition 354 Scientists, Bengal Fan. Proceedings of the International Ocean Discovery Program, 354: College Station, TX (International Ocean Discovery Program). https://doi.org/10.14379/iodp.proc.354.203.2020

Poppe, L.J., Paskevich, V.F., Hathaway, J.C., and Blackwood, D.S., 2001. A laboratory manual for X-ray powder diffraction. USGS Open-File Report, 2001-41. http://pubs.er.usgs.gov/publication/ofr0141

Rapuc, W., Bouchez, J., Sabatier, P., Genuite, K., Poulenard, J., Gaillardet, J., and Arnaud, F., 2021. Quantitative evaluation of human and climate forcing on erosion in the alpine Critical Zone over the last 2000 years. Quaternary Science Reviews, 268:107127. https://doi.org/10.1016/j.quascirev.2021.107127

Ray, S., Gault, H.R., and Dodd, C.G., 1957. The separation of clay minerals from carbonate rocks. American Mineralogist, 42(9–10):681–686.

Wilson, D.J., Piotrowski, A.M., Galy, A., and Clegg, J.A., 2013. Reactivity of neodymium carriers in deep sea sediments: Implications for boundary exchange and paleoceanography. Geochimica et Cosmochimica Acta, 109:197–221. https://doi.org/10.1016/j.gca.2013.01.042